

Research Paper

# Cholesterol Overload Drives Hepatic Steatosis by Inhibiting OGT-dependent PPAR $\alpha$ O-GlcNAcylation and Transactivation

Rui Guo<sup>1,2#</sup>, Yanhui Li<sup>1#</sup>, Qinchao Ding<sup>2</sup>, Chad Slawson<sup>3</sup>, Udayan Apte<sup>4</sup>, Yuwei Jiang<sup>5</sup>, Xiaobing Dou<sup>6</sup>, Songtao Li<sup>2</sup>, Zhenyuan Song<sup>1</sup>✉

1. Department of Kinesiology and Nutrition, University of Illinois Chicago, Chicago, IL, USA.
2. School of Public Health, Zhejiang Chinese Medical University, Hangzhou, Zhejiang, PR. China.
3. Department of Biochemistry and Molecular Biology, Kansas University Medical Center, Kansas City, KS, USA
4. Department of Pharmacology, Toxicology & Therapeutics, Kansas University Medical Center, Kansas City, KS, USA
5. Department of Physiology & Biophysics, University of Illinois Chicago, Chicago, IL, USA
6. School of Life Science, Zhejiang Chinese Medical University, Hangzhou, Zhejiang, PR. China.

# These authors equally contributed to this work.

✉ Corresponding author: Zhenyuan Song, PhD, Phone: (312)-996-7892, Fax: (312)-413-0319, E-mail: song2008@uic.edu.

© The author(s). This is an open access article distributed under the terms of the Creative Commons Attribution License (<https://creativecommons.org/licenses/by/4.0/>). See <https://ivyspring.com/terms> for full terms and conditions.

Received: 2026.03.25; Accepted: 2026.04.22; Published: 2026.05.18

## Abstract

Although dietary cholesterol is known to exacerbate liver disease progression, whether and how it contributes to hepatic steatosis, the hallmark early pathological feature of both MASLD and ALD, remains poorly understood. Here, we investigated how cholesterol disrupts hepatic triacylglycerol metabolism using both dietary and cellular cholesterol-loading models. Integrated transcriptomic, metabolomic, and biochemical analyses were performed, and causality was examined through genetic and pharmacologic modulation in multiple hepatocyte systems and mice. Our results demonstrate that cholesterol overload induces hepatocellular fat accumulation in a dose-dependent, cell-autonomous manner, primarily by suppressing fatty acid  $\beta$ -oxidation. Mechanistically, we identified PPAR $\alpha$  inhibition as a key event underlying this effect. Cholesterol overload suppressed PPAR $\alpha$  transactivation, thereby impairing fatty acid  $\beta$ -oxidation and promoting hepatocellular fat accumulation. This inhibition was mechanistically linked to reduced O-GlcNAcylation. Specifically, cholesterol overload downregulated OGT, leading to reduced protein O-GlcNAcylation and consequent PPAR $\alpha$  inhibition; similarly, liver-specific OGT knockout mice exhibited suppressed PPAR $\alpha$  activity and increased hepatic fat accumulation. RNA-sequencing and co-immunoprecipitation analyses identified PPAR $\alpha$  as an O-GlcNAc-modified protein, and loss of this modification impaired its transactivity. Functionally, restoration of O-GlcNAcylation via genetic OGA knockdown or pharmacological activation of PPAR $\alpha$  with WY14643 alleviated cholesterol-induced hepatic steatosis in mice without altering hepatic cholesterol levels. Lastly, we identified SREBP2 as the upstream transcriptional regulator linking cholesterol overload to OGT suppression. In conclusion, our findings in this study uncover a previously unrecognized cholesterol-OGT-PPAR $\alpha$  axis that suppresses hepatic fatty acid  $\beta$ -oxidation and drives steatosis. Targeting O-GlcNAc cycling or activating PPAR $\alpha$  represents a promising therapeutic strategy for MASLD.

Keywords: hepatic steatosis, cholesterol, O-GlcNAcylation, OGT, PPAR $\alpha$ 

## Introduction

Metabolic dysfunction-associated steatotic liver disease (MASLD) has become the most common chronic liver disorder worldwide, encompassing a spectrum from simple steatosis to steatohepatitis,

fibrosis, and cirrhosis [1-3]. Its rising prevalence parallels increasing rates of obesity, insulin resistance, and Western dietary habits [4-6]. Among dietary factors, cholesterol has emerged as an important

contributor to MASLD progression. A growing body of clinical and experimental evidence demonstrates that cholesterol-enriched diets exacerbate hepatic inflammation, injury, and fibrogenic response, thereby accelerating MASLD progression [7-9]. Intriguingly, despite its well-established role in promoting disease progression, it remains unclear whether and how cholesterol drives hepatic steatosis, the defining feature of early-stage MASLD, particularly given that cholesterol itself is not a direct substrate for triacylglycerol synthesis.

Peroxisome proliferator-activated receptor alpha (PPAR $\alpha$ ) is a ligand-activated nuclear receptor abundantly expressed in hepatocytes, where it orchestrates transcriptional programs that regulate lipid catabolism and energy homeostasis [10-12]. Upon activation, PPAR $\alpha$  induces genes involved in mitochondrial and peroxisomal  $\beta$ -oxidation, ketogenesis, and lipoprotein metabolism, thereby facilitating fatty acid clearance and maintaining hepatic metabolic integrity [13-16]. In MASLD, reduced PPAR $\alpha$  activity is a consistent molecular feature associated with hepatic steatosis, inflammation, and disease progression [11, 15, 17-19]. Experimental evidence indicates that genetic ablation or pharmacological inhibition of PPAR $\alpha$  suppresses fatty acid oxidation, promotes lipid accumulation, and increases susceptibility to diet-induced liver injury [19-21]. Conversely, activation with selective agonists such as WY14643 or fenofibrate alleviates steatosis, inflammation, and fibrotic remodeling, underscoring the pivotal role of PPAR $\alpha$  in protecting against MASLD pathogenesis [22-25]. Protein O-GlcNAcylation is a dynamic and reversible post-translational modification in which O-linked N-acetylglucosamine (O-GlcNAc) is added to serine or threonine residues of nuclear and cytoplasmic proteins [26-28]. This process is catalyzed by O-GlcNAc transferase (OGT) and removed by O-GlcNAcase (OGA), using UDP-GlcNAc generated through the hexosamine biosynthetic pathway (HBP) as the donor substrate [27, 29]. Because HBP integrates inputs from glucose, glutamine, acetyl-CoA, and nucleotide metabolism, O-GlcNAcylation functions as a nutrient-sensing mechanism that couples cellular metabolic status to signaling and transcriptional regulation [30, 31]. Accumulating evidence supports that dysregulated hepatic O-GlcNAcylation contributes to the development of multiple liver diseases, including MASLD, steatohepatitis, fibrosis, and hepatocellular carcinoma [32-35]; however, current findings remain contradictory. On the one hand, several studies have reported that a high-fat diet (HFD) or metabolic overload elevates hepatic protein O-GlcNAcylation, either by enhancing *de novo*

lipogenesis or by upregulating CD36, thereby accelerating the progression from MASLD to steatohepatitis (MASH) [30, 36-38]. On the other hand, it has been clearly demonstrated that hepatocyte-specific OGT knockout mice exhibit profound metabolic and structural abnormalities, including increased liver injury, inflammation, fibrosis, and exacerbated development of DEN-induced hepatocellular carcinoma [39, 40]. These opposing observations suggest that basal O-GlcNAcylation is essential for maintaining hepatic homeostasis and function, underscoring the complex and context-dependent role of O-GlcNAc signaling in liver metabolism. Therefore, it is imperative to clarify how nutrient or lipid overload, including cholesterol loading, modulates OGT-mediated O-GlcNAcylation and contributes to the initiation and progression of MASLD.

To elucidate whether and how cholesterol loading affects hepatocellular lipid metabolism, we employed integrated *in vitro* and *in vivo* approaches and identified a previously unrecognized cholesterol-OGT-PPAR $\alpha$  signaling axis that mechanistically links free cholesterol accumulation to hepatocellular fat accumulation. We demonstrate that cholesterol overload induces hepatic steatosis by inhibiting PPAR $\alpha$  activity via suppression of OGT-dependent protein O-GlcNAcylation. Free cholesterol, but not cholesteryl esters, downregulates OGT expression, leading to reduced global O-GlcNAcylation, including modification of PPAR $\alpha$ , thereby impairing its transcriptional control of fatty acid  $\beta$ -oxidation and promoting lipid accumulation. Importantly, restoring O-GlcNAcylation or activating PPAR $\alpha$  reverses cholesterol-induced steatosis, establishing a mechanistic cholesterol-OGT-O-GlcNAc-PPAR $\alpha$  axis that represents a targetable pathway in MASLD development.

## Materials and Methods

### Reagents

Chemicals, including bovine serum albumin (BSA, A7030) and DMSO (D2650), were purchased from Sigma-Aldrich. Other chemicals used in this study were purchased as follows: Simvastatin (Adipogen, AG-CN2-0052), Low density lipoprotein (ThermoFisher, L3486), Cholesterol-water soluble (MCE, HY-N0322A), Etomoxir (MCE, HY-50202A), Pirinixic acid (MCE, HY-16995), Fenofibrate (MCE, HY-17356), Methyl- $\beta$ -cyclodextrin (MCE, HY-101461), OSMI-1 (MCE, HY-119738), Thiamet G (MCE, HY-12588), Protein A/G PLUS-Agarose (Santa Cruz, sc-2003), Normal mouse IgG (Santa Cruz, sc-2025), and NP-40 alternative (Santa Cruz, CAS 9016-45-9).

## Cell culture

Murine AML12 and human HepG2 hepatocyte cell lines were obtained from the American Type Culture Collection (ATCC, VA, USA). Human hepatoma HepaRG cells (Thermo Fisher Scientific, HPRGC10), which are terminally differentiated and non-proliferative, were also used in this study. (See **supplementary information** for details).

## RNA interference

Cultured cells were transfected with *Ogt* siRNA (Invitrogen, 173150), *Soat2* (Invitrogen, 101666), and *Srebf2* (Invitrogen, 284040) using Lipofectamine 2000 (Invitrogen, 3016547) based on the manufacturer's instructions. Cells in the control group were transfected with scrambled siRNA (Santa Cruz, sc-37007). (See **supplementary information** for details).

## Fatty acid oxidation (FAO) staining

FAO activity was measured using the FAOBlue™ detection reagent (Funakoshi, FDV-0033). (See **supplementary information** for details).

## Bodipy staining

Cells ( $1 \times 10^5$ ) were seeded into 24-well plates and cultured for 16 hours. After treatment, cells were washed with PBS, fixed in 4% formaldehyde (Pierce, Rockford, IL) for 15 min, and rinsed again. 5  $\mu$ M BODIPY 493/503 (Invitrogen, D3922) was applied for 15 min at room temperature. Following PBS washes, nuclei were counterstained with DAPI mounting medium (Sigma-rich, Saint Louis, MO). Images were captured using a LEICA inverted fluorescence microscope.

## Animal experiments

All mice were housed under specific pathogen-free (SPF) conditions, with controlled temperatures (18-23 °C), humidity (40-60%), and a 12-hour light/dark cycle. Mice had free access to food and water throughout the study. All animal studies were approved by the Institutional Animal Care and Use Committee at the University of Illinois Chicago and were conducted in accordance with the NIH Guide for the Care and Use of Laboratory Animals. Ten-week-old male C57BL/6 mice were used for dietary interventions with varying cholesterol concentrations (Sigma Grade,  $\geq 99\%$ , Sigma-Aldrich, C8667) and for pharmacological treatment with the PPAR $\alpha$  agonist WY14643. In addition, ten-week-old male C57BL/6 mice were subjected to hepatic OGA knockdown using adeno-associated virus serotype 8 (AAV8)-mediated shRNA delivery. Mice received either AAV8-sh*Oga* or AAV8-shScrmB control via orbital injection during dietary intervention on day 10. Animals were

maintained on a 2% cholesterol diet for 30 days after viral administration. (See **supplementary information** for details).

## Histological analysis

Liver tissues were fixed in 10% neutral-buffered formalin for 24 hours. Selected samples were embedded in paraffin, sectioned at 4  $\mu$ M, and stained with hematoxylin and eosin (H&E) for histological evaluation. To assess collagen deposition, paraffin-embedded liver sections were stained with Sirius Red (G-Clone, Beijing, China) according to standard protocols. For lipid staining, portions of the liver were embedded in Tissue-Tek OCT compound (Sakura, Tokyo, Japan), frozen, sectioned at 8  $\mu$ M, and stained with Oil Red O. Images were captured by a Zeiss Axio Observer A1 inverted microscope (Oberkochen, Germany).

## Biochemical assays

Hepatic and plasma triacylglycerol (TAG) and total cholesterol (TC) contents, as well as cellular lipid levels, were quantified using standard biochemical assays with commercial reagent kits (Jiancheng, Nanjing, China) according to the manufacturers' instructions. Cellular TAG and TC levels were normalized to protein content. (See **supplementary information** for details).

## Chromatin immunoprecipitation analysis (ChIP)

ChIP assays were performed using the Pierce™ Agarose ChIP Kit (Thermo Fisher, Rockford, IL, USA) according to the manufacturer's protocol. HepG2 cells were cultured in 6-well plates and treated with vehicle (UT), 4  $\mu$ M cholesterol, or 10  $\mu$ M simvastatin for 12 hours. Cells ( $\sim 2 \times 10^6$  per condition) were crosslinked in culture by adding formaldehyde to a final concentration of 1% for 10 min at room temperature, and the reaction was terminated with glycine. Chromatin was enzymatically fragmented and immunoprecipitated with an antibody specific to SREBF2. DNA was purified from immunoprecipitants and analyzed by quantitative PCR. The target region encompasses the *Ogt* gene promoter on chromosome X, and the primers were designed to amplify a fragment containing the predicted SREBF2 binding site. The primer sequences were:

Forward: 5'-GGTTGGTGCTCAATTTTCAGGA-3';

Reverse: 5'-GCTACCTAGCCCCTTCACTAC-3'.

## Co-immunoprecipitation (Co-IP)

Co-IP was performed using AML12 cells to assess protein interactions involving PPAR $\alpha$ . Briefly, cells

were lysed in ice-cold NP-40 lysis buffer (150 mM NaCl, 50 mM Tris-HCl, 1% NP-40, pH 7.8) supplemented with a mammalian protease inhibitor cocktail. Equal amounts of protein lysates (200 µg) were incubated overnight at 4 °C with anti-PPAR $\alpha$  antibody (or normal mouse IgG as a negative control) on a nutating platform. Antibody-protein complexes were captured using Protein A/G agarose beads (Santa Cruz Biotechnology) for 1 hour at 4 °C with gentle agitation. Beads were washed four times with lysis buffer, and bound proteins were eluted by boiling in SDS loading buffer. Eluates were resolved by SDS-PAGE and analyzed by Western blot for O-GlcNAcylated proteins and OGT.

### RNA sequencing and data analysis

For *in vivo* RNA sequencing (RNA-seq), total RNA was extracted using TRIzol® reagent (Invitrogen) from three control (Ctrl) and three 2% cholesterol (Chol) mouse liver samples. *In vitro* RNA-seq was also performed in AML12 cell experiments: untreated (UT, n=3) and M $\beta$ CD-cholesterol-treated (4 µM, n=4) cells. Library preparation and sequencing were conducted on the Illumina NovaSeq 6000 platform by Shanghai Majorbio Bio-Pharm Technology Co., Ltd. Bioinformatic analyses, including differential expression and functional enrichment, were performed using the Majorbio I-Sanger Cloud Platform (<https://www.i-sanger.com>). (See **supplementary information** for details).

### Quantitative real-time polymerase chain reaction (qRT-PCR)

Total RNA was extracted using TRIzol® reagent

(Invitrogen, Carlsbad, CA) and reverse-transcribed into cDNA with kits from Promega (Madison, WI), following the manufacturer's instructions. qPCR was performed in 384-well plates using SYBR Green/ROX qPCR Master Mix (2X) on an Applied Biosystems 7300 Real-Time PCR System (Thermo Fisher Scientific). Gene expression levels were normalized to 18s rRNA and calculated using the  $2^{-\Delta\Delta Ct}$  method. Primers were synthesized by IDT, and their sequences are listed in **Table 1**.

### PPAR $\alpha$ transcription factor activity

Nuclear extracts (Thermo Scientific, 78833) from cells and tissues were prepared using a nuclear extraction kit according to the manufacturer's instructions. (See **supplementary information** for details).

### Metabolomics analysis

Targeted metabolomic analysis of central carbon metabolism was performed using ultra-performance liquid chromatography coupled with tandem mass spectrometry (UPLC-MS/MS; Thermo Fisher Scientific). Liver tissues were extracted using a methanol/water (80:20, v/v) solution containing internal standards, and metabolites were quantified by multiple reaction monitoring. Data acquisition and processing were carried out by Shanghai Majorbio Bio-Pharm Technology Co., Ltd. using in-house databases and the Majorbio cloud platform (<https://cloud.majorbio.com>). (Please refer to **the Supplementary information** for details.)

**Table 1.** The sequences of all primers.

Target genes	Forward primer (5' to 3' )	Reverse primer (5' to 3' )
Mouse <i>Oga</i>	GGGTTATGGAGCAGAGAAAAGAG	CCTGGCGAAATAGCATAGATGAA
Mouse <i>Ogt</i>	GACGCAACCAAACCTTTCAGT	TCAAGGGTGACAGCCTTTTCA
Mouse <i>Soat2</i>	ACAAGACAGACCTCTCCCTC	ATGGTTCGAAATGTTGCACC
Mouse <i>Fasn</i>	GGAGGTTGGTATAGCCGGTAT	TGGGTAATCCATAGAGCCAG
Mouse <i>Acaca</i>	GATGAACCATCTCCGTTGGC	GACCCAATTATGAATCGGGAGTG
Mouse <i>Acly</i>	CAGCCAAGGCAATTCAGAGC	CTCGACGTTGATTAACCTGGTCT
Mouse <i>sreb1</i>	GCAGCCACCATCTAGCCTG	CAGCAGTGAGTCTGCCTTGAT
Mouse <i>sreb2</i>	CAGGTGCAGACGGTACAGG	CGACCCCTACTGGCACTTGAA
Mouse <i>Ppara</i>	AGAGCCCCATCTGTCCTCTC	ACTGGTAGTCTGCAAAAACCAA
Mouse <i>Hmgcs2</i>	GAAGAGAGCGATGCAGGAAAC	GTCCACATATTGGGCTGGAAA
Mouse <i>Cpt1a</i>	CTCCGCTGAGCCATGAAG	CACCAGTGATGATGCCATTCT
Mouse <i>Acox1</i>	TCCGACTTCCAACATGAGGA	CTGGGCGTAGGTGCCAATTA
Mouse <i>Cyp7a1</i>	GGGATTGCTGTGGTAGTGAGC	GGTATGGAATCAACCCGTGTCT
Mouse <i>Gp1</i>	GAAGCCAACGCCTGCAAAAATC	CCAACGGGTATGAGCTATTCC
Mouse <i>Gnpnat1</i>	ATGAAAACCCGATGAAACTCCC	GCCTCAAAAACCAAGCCTTCTC
Mouse <i>Uap1</i>	CCATCCCCCGCTTGAAAGAT	CCCTCTCCAGCATAAGAGATGA
Mouse <i>18s</i>	TAACCCGTTGAACCCCAT	CCATCCAATCGGTAGTAGCC

## Western blot analysis

Cells and liver tissues were lysed in RIPA buffer containing protease/phosphatase inhibitors (Beyotime, China). Equal amounts of protein (~30 µg) were separated by SDS-PAGE and transferred to membranes. Standard immunoblotting was performed with primary antibodies and IRDye-conjugated secondary antibodies (LI-COR), and signals were quantified using the Odyssey CLx system. For detection of N-linked glycosylation, membranes were probed with concanavalin A (ConA, Sigma-Aldrich) and visualized by chemiluminescence (ECL). β-actin and Lamin B1 served as loading controls. (Please refer to the **Supplementary information** for details on the sources and catalog numbers of all specific antibodies.)

## Statistical analysis

All statistical analyses were performed using GraphPad Prism (version 9.0; GraphPad Software, San Diego, CA). Unless otherwise specified, experiments were independently repeated at least three times ( $n \geq 3$ ). Data are expressed as mean  $\pm$  standard deviation (SD). For comparisons between two groups, normality of data distribution was first evaluated using the *Shapiro-Wilk* test. Normally distributed data were analyzed by a two-tailed unpaired Student's *t*-test, whereas non-normally distributed data were assessed using the *Mann-Whitney U* test. For comparisons among more than two groups, one-way analysis of variance (ANOVA) followed by *Tukey's post hoc* test was applied. When two independent variables were involved, a two-way ANOVA with *Sidak's post hoc* analysis was used. For nonparametric data across multiple groups, the *Kruskal-Wallis* test was followed by *Dunn's* multiple comparison test. Sample sizes and *p*-values are represented by individual data points in bar-scatter plots. A *p*-value  $< 0.05$  was considered statistically significant.

## Results

**Hepatocellular cholesterol overload promotes hepatic steatosis.** Both *in vivo* and *in vitro* studies were conducted to evaluate the effect of cholesterol overload on hepatic fat (triacylglycerol, TAG) accumulation. *In vivo*, 10-week-old male C57BL/6 mice were fed a standard chow diet with or without 2% (w/w) cholesterol for 4 weeks. As shown in **Fig. 1**, cholesterol supplementation did not alter body weight gain (**Fig. 1A**) but significantly increased liver mass

(**Fig. 1B**), leading to a significant increase in the liver-to-body weight ratio (**Fig. 1C**). As expected, hepatic total cholesterol (TC) content was markedly elevated (**Fig. 1D**). Importantly, dietary cholesterol supplementation induced hepatic steatosis, evidenced by increased hepatic TAG levels (**Fig. 1E**) and confirmed by histological staining (**Fig. 1F**).

To test whether cholesterol-induced hepatic TAG accumulation occurs through cell-autonomous mechanisms, we next examined the effects of cholesterol loading in cultured hepatocytes. AML12 cells, a non-transformed murine hepatocyte line, were first used, and key findings were validated in HepG2 and differentiated HepaRG cells to ensure translational relevance. In AML12 cells, treatment with methyl-β-cyclodextrin (MβCD)-complexed cholesterol significantly increased cellular TC (**Fig. 1G**) and TAG levels (**Fig. 1H**), as confirmed by BODIPY 493/503 staining (**Fig. 1I**). MβCD alone had no effect (**Figs. S1A, B**), ruling out vehicle artifacts. Similar results were observed in HepaRG (**Figs. 1J, K**) and HepG2 (**Figs. S1C-E**) cells, indicating a conserved, cell-autonomous effect of cholesterol loading. Moreover, pharmacological inhibition of endogenous cholesterol synthesis with simvastatin (10 µM) markedly reduced cholesterol-induced increases in cellular TC and TAG (**Figs. 1L-N**) in AML12 cells, with comparable effects in HepG2 cells (**Figs. S1F-H**). These findings confirm that elevated cellular cholesterol directly drives hepatocellular fat accumulation.

In hepatocytes, cholesterol exists in both free and esterified forms, with cholesteryl esters synthesized by acyl-CoA: cholesterol acyltransferase 2 (ACAT2, encoded by *Soat2*). To determine which pool contributes to TAG accumulation, *Soat2* was silenced in AML12 cells using siRNA (**Fig. 1O**). Remarkably, ACAT2 knockdown further enhanced MβCD-cholesterol-induced TAG accumulation (**Fig. 1P**), a result that was reproduced in HepG2 cells (**Fig. S1I**). These findings indicate that free cholesterol, rather than esterified cholesterol, is the major driver of lipid droplet formation, while ACAT2-mediated esterification serves a protective buffering role against free cholesterol-induced lipotoxicity. To assess physiological relevance, AML12 and HepG2 cells were treated with increasing concentrations of low-density lipoprotein (LDL, 0-50 µg/mL) for 16 hours. LDL supplementation dose-dependently increased cellular TC and TAG levels in both cell types (**Figs. 1Q, R, and Figs. S1J, K**), confirming that exogenous cholesterol promotes hepatocellular fat accumulation.

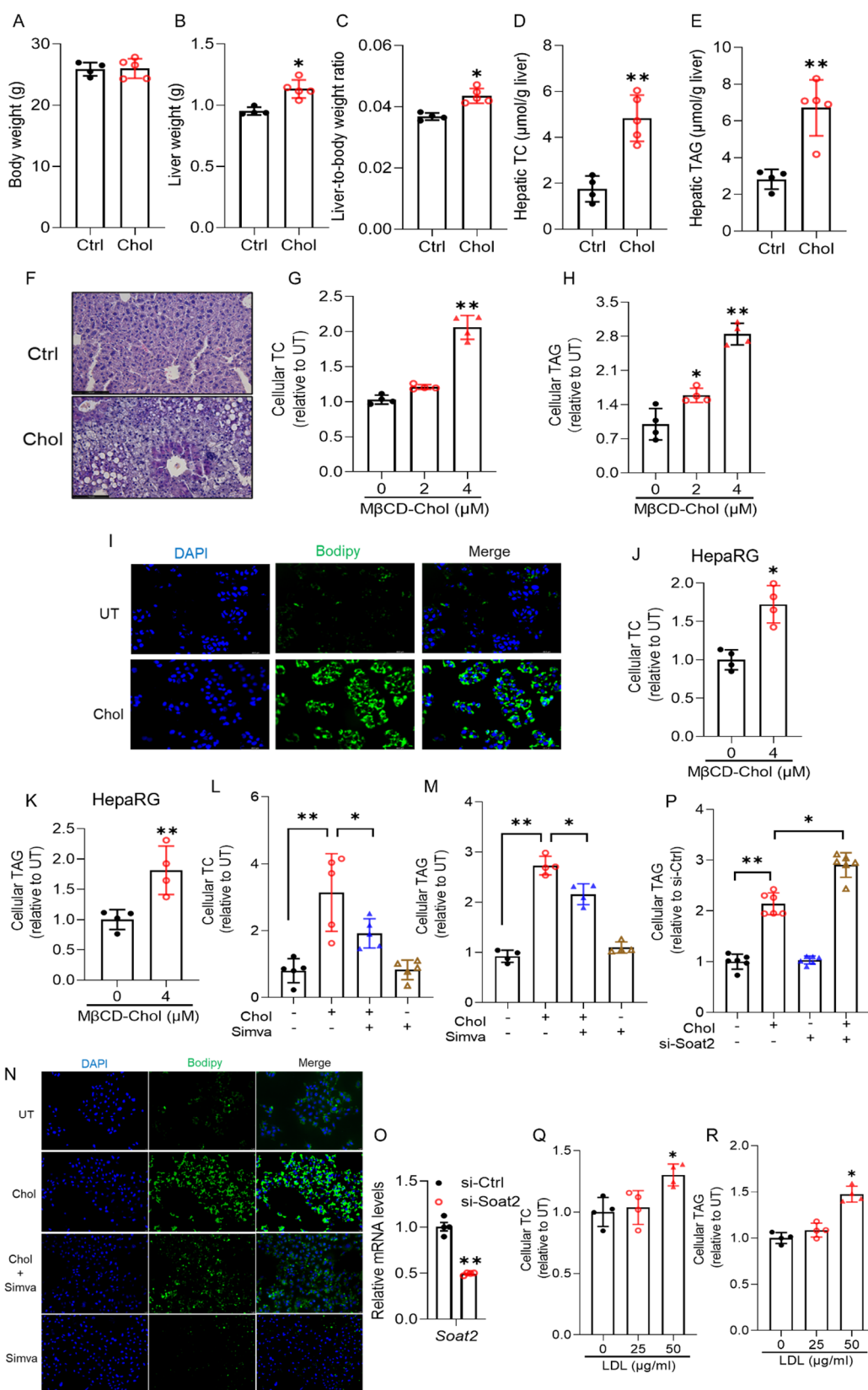


**Figure 1. Hepatocellular cholesterol overload promotes hepatic steatosis.** Male C57BL/6j mice (10-week-old) were fed with a chow diet supplemented with and without cholesterol (2%, w/w) for 4 weeks. (A) body weight; (B) liver weight; (C) liver-to-body weight ratio; (D) hepatic total cholesterol (TC) content; (E) hepatic triacylglycerol (TAG) content; (F) representative histology examination (H&E, Oil Red O, and Sirius Red staining). AML12 cells were treated with methyl- $\beta$ -cyclodextrin (M $\beta$ CD)-complexed cholesterol for 16 hours. (G) cellular total cholesterol (TC); (H) cellular TAG; (I) BODIPY staining (493/503), scale bar=50  $\mu\text{m}$ . HepaRG cells were treated with methyl- $\beta$ -cyclodextrin (M $\beta$ CD)-complexed cholesterol for 16 hours. (J) cellular TC; (K) cellular TAG. AML12 cells were pretreated with simvastatin (10  $\mu\text{M}$ ) for 2 hours before M $\beta$ CD-cholesterol loading. (L) cellular TC; (M) cellular TAG; (N) BODIPY staining (493/503). Scale bar=1  $\mu\text{m}$ . AML12 cells were transfected with Soat2 siRNA overnight prior to M $\beta$ CD-cholesterol loading. (O) *Soat2* mRNA; (P) cellular TAG. AML12 cells were treated with LDL (0-50  $\mu\text{g/mL}$ ) for 16 hours. (Q) cellular TC; (R) cellular TAG. Chol, cholesterol; M $\beta$ CD-chol, M $\beta$ CD-cholesterol; LDL, low-density lipoprotein; Simva, simvastatin. \* $P < 0.05$  and \*\* $P < 0.01$  represent statistical difference.

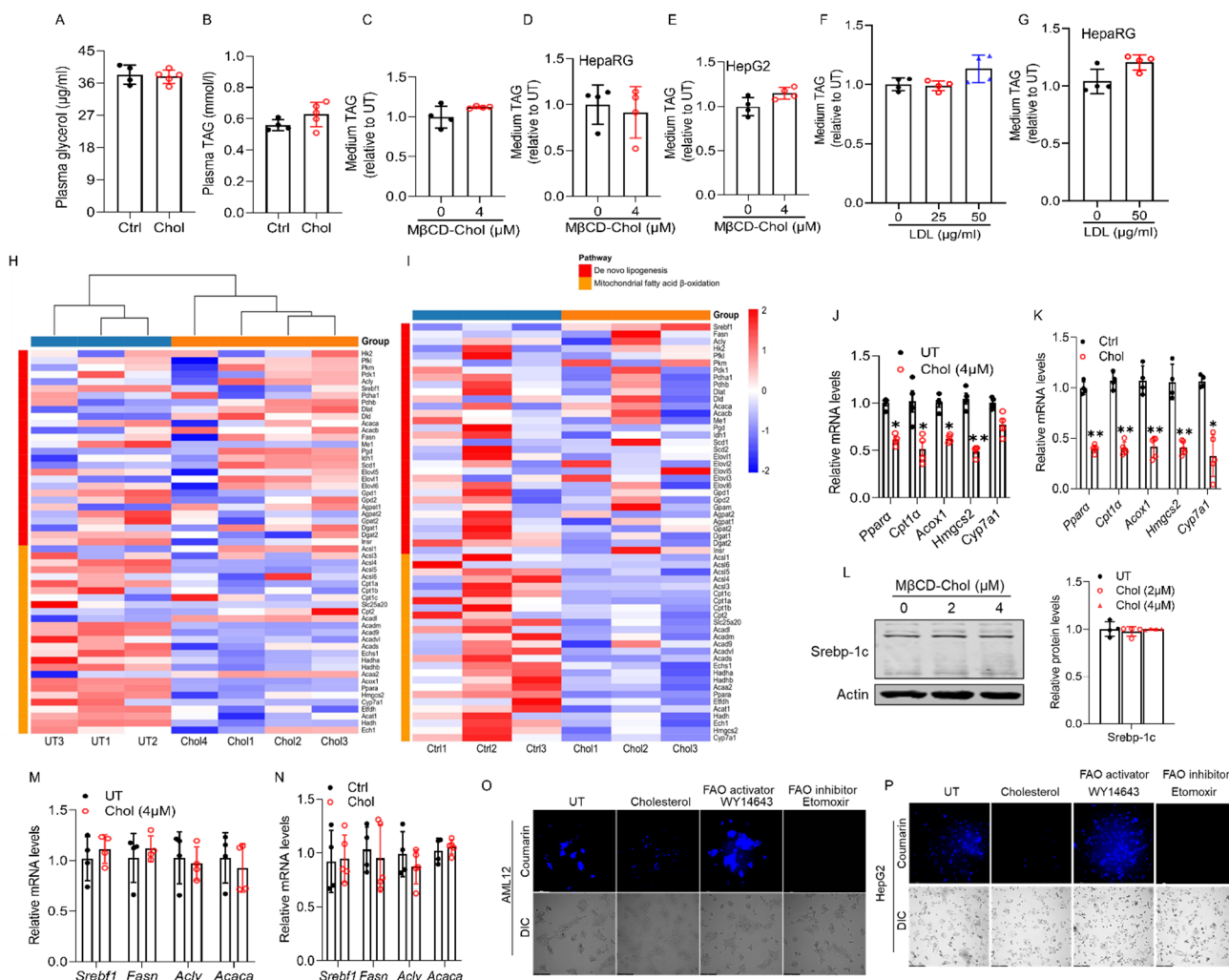


**Figure 2. Impaired mitochondrial fatty acid β-oxidation is a key metabolic defect contributing to cholesterol-induced hepatocellular fat accumulation.** (A, B) Plasma glycerol and TAG levels in chow-fed mice supplemented with and without 2% cholesterol (w/w) for 4 weeks. (C-E) Extracellular TAG concentrations in the culture medium of AML12, HepaRG, and HepG2 cells following cholesterol. (F, G) Extracellular TAG concentrations in the culture medium of AML12 and HepG2 cells following LDL supplementation. (H, I) Heatmap visualization of representative lipid-related pathways in AML12 cells and *in vivo*. (J, K) qRT-PCR validation of mitochondrial fatty acid β-oxidation (*Ppara*, *Cpt1a*, *Acox1*, *Hmgcs2*, and *Cyp7a1*) *in vitro* and *in vivo*. (L-N) Unaltered SREBP-1c pathway activation in AML12 cells following cholesterol exposure and in chow-fed mice supplemented with and without 2% cholesterol for 4 weeks, tested by Western-blot and qRT-PCR. (O, P) Fluorescence-based FAOBlue™ assay of fatty acid β-oxidation capacity (FAO) in AML12 and HepG2 cells after cholesterol loading (4 µM, 16 h). (40× objective). Chol, cholesterol; MβCD-chol, MβCD-cholesterol; LDL, low-density lipoprotein. \*P < 0.05 and \*\*P < 0.01 represent statistical significance.

**Impaired fatty acid β-oxidation is a key metabolic defect contributing to cholesterol-induced hepatocellular fat accumulation.** Excessive hepatic fat accumulation may result from multiple metabolic disturbances, including enhanced *de novo* lipogenesis (DNL), impaired mitochondrial β-oxidation, increased fatty acid influx from adipose tissue, or defective very low-density lipoprotein (VLDL) secretion [41, 42]. In mice fed a cholesterol-enriched diet, plasma glycerol levels remained unchanged (Fig. 2A), excluding enhanced adipose lipolysis as a contributing factor. Moreover, a modest SREBP-1c elevation in plasma TAG levels was observed (Fig. 2B), suggesting that hepatic TAG accumulation was not attributable to impaired VLDL exports. Consistently, cholesterol loading, via either

MβCD-cholesterol or LDL exposure, did not affect extracellular TAG levels in AML12, HepaRG, or HepG2 cells (Figs. 2C-G), further indicating that VLDL secretion was preserved. To define how cholesterol promotes hepatic lipid accumulation, we conducted RNA-seq in cholesterol-treated AML12 cells (4 µM) and in the livers of mice fed a 2% (w/w) cholesterol diet for 4 weeks. Transcriptomic analysis showed that cholesterol did not alter the expression of DNL-related genes but markedly suppressed mitochondrial fatty acid β-oxidation genes in both models (Figs. 2H, I). These findings were confirmed by qRT-PCR in both settings (Figs. 2J, K). The lack of changes in mature SREBP-1c protein levels *in vitro* and *in vivo* after cholesterol loading (Figs. 2L-N) further

supports that cholesterol-induced lipid accumulation occurs independently of DNL activation. In contrast, consistent with the transcriptomic downregulation of fatty acid  $\beta$ -oxidation genes, fluorescence-based assessment of fatty acid oxidation using the FAOBlue™ assay demonstrated that cholesterol exposure markedly impaired mitochondrial  $\beta$ -oxidation in both AML12 and HepG2 cells (Figs. 2O, P). Collectively, these findings establish that defective mitochondrial  $\beta$ -oxidation, rather than enhanced lipogenesis or impaired VLDL export, is the principal mechanism driving cholesterol-induced hepatic TAG accumulation.

**Hepatocellular free cholesterol overload suppresses PPAR $\alpha$  signaling, contributing to intracellular lipid accumulation.** One of the key regulators of hepatic fatty acid  $\beta$ -oxidation is PPAR $\alpha$ . Our RNA-sequencing analysis revealed that its expression is downregulated in the liver following cholesterol-enriched diet feeding (Figs. 2H-K). We therefore next examined whether cholesterol impairs hepatic PPAR $\alpha$  signaling. Western blot analysis revealed a pronounced reduction in PPAR $\alpha$  protein abundance in the livers of mice fed a cholesterol-enriched diet (Fig. 3A) and in cultured hepatocytes treated with cholesterol (Figs. 3B, C, and Fig. S2A). Consistently, hepatic PPAR $\alpha$  transcriptional activity, measured using an ELISA-based assay, was significantly diminished in both cholesterol-fed mice (Fig. 3D) and cholesterol-treated AML12 cells (Fig. 3E). Similar inhibitory effects were also observed in AML12 cells treated with LDL (Figs. S2B, C). Notably, *Soat2* knockdown further exacerbated cholesterol-induced repression of PPAR $\alpha$  target genes (Fig. 3F), implicating the accumulation of free cholesterol as a key driver of PPAR $\alpha$  inhibition. Conversely, simvastatin (10  $\mu$ M) pretreatment restored PPAR $\alpha$  expression and activation of its target genes (Fig. 3G), as well as rescued fatty acid  $\beta$ -oxidation inhibition, determined by FAOBlue staining, in cultured hepatocytes (Fig. 3H and Fig. S2D). To determine whether PPAR $\alpha$  activation mechanistically contributes to cholesterol-induced hepatocellular fat accumulation, we conducted rescue experiments using selective PPAR $\alpha$  agonists in cultured hepatocytes. In cholesterol-loaded AML12 cells, activation of PPAR $\alpha$  with WY14643 (10  $\mu$ M) or fenofibrate (20  $\mu$ M) markedly attenuated intracellular fat accumulation (Fig. 3I). In contrast, inhibition of mitochondrial fatty acid  $\beta$ -oxidation with etomoxir (20  $\mu$ M) further exacerbated TAG accumulation under the

same conditions (Fig. 3J). As a result, BODIPY staining revealed fewer lipid droplets in WY14643-treated cells, whereas etomoxir treatment intensified lipid deposition (Fig. 3K).

**Cholesterol loading downregulates hepatic OGT expression and suppresses hepatic protein O-GlcNAcylation.** We previously demonstrated that activation of the hexosamine biosynthetic pathway (HBP) is essential for glucose-induced hepatic TAG accumulation [43], underscoring its central role in hepatic lipid metabolism. Transcriptomic profiling of liver tissues from cholesterol-fed mice revealed a selective downregulation of *Ogt* (Fig. 4A), which encodes O-linked N-acetylglucosamine transferase (OGT), the sole enzyme catalyzing protein O-GlcNAcylation using the HBP-derived substrate UDP-GlcNAc. This suppression was highly specific, as expression of other core HBP enzymes (*Gfpt1*, *Gnpnat1*, *Uap1*) and *Oga* (encoding O-GlcNAcase) remained unchanged (Fig. 4A). Subsequent qRT-PCR and Western blot analyses confirmed these transcriptomic findings. In cholesterol-fed mouse livers, OGT expression was significantly reduced at both the mRNA (Fig. 4B) and protein levels, accompanied by a marked decrease in global protein O-GlcNAcylation (Fig. 4C and Fig. S3A), while N-linked glycosylation remained unchanged (Fig. 4D and Fig. S3B). Similarly, in AML12 hepatocytes, cholesterol loading with M $\beta$ CD-cholesterol (4  $\mu$ M) markedly suppressed OGT gene expression (Fig. 4E), without affecting other HBP enzymes. This was associated with a parallel reduction in global protein O-GlcNAcylation (Fig. 4F and Fig. S3C) but no change in N-linked glycosylation (Fig. 4G and Fig. S3D). Consistent results were observed in HepaRG and HepG2 cells (Fig. 4H and Figs. S3E, F). Notably, pharmacological depletion of intracellular cholesterol with simvastatin restored OGT expression and normalized protein O-GlcNAcylation in cultured hepatocytes (Fig. 4I and Figs. S3G, H). Comparable rescue effects were observed when LDL served as the cholesterol source (Figs. 4J, K, and Fig. S3I). Moreover, *Soat2* knockdown, which increases free cholesterol levels, further reduced OGT expression and exacerbated O-GlcNAcylation loss (Figs. 4L, M, and Fig. S3J), reinforcing free cholesterol as the primary mediator of this effect. Consistent with these molecular findings, targeted metabolomics revealed that dietary cholesterol supplementation significantly reduced hepatic levels of glucosamine-6-phosphate and N-acetyl-D-glucosamine, two key intermediates in the HBP (Fig. 4N).

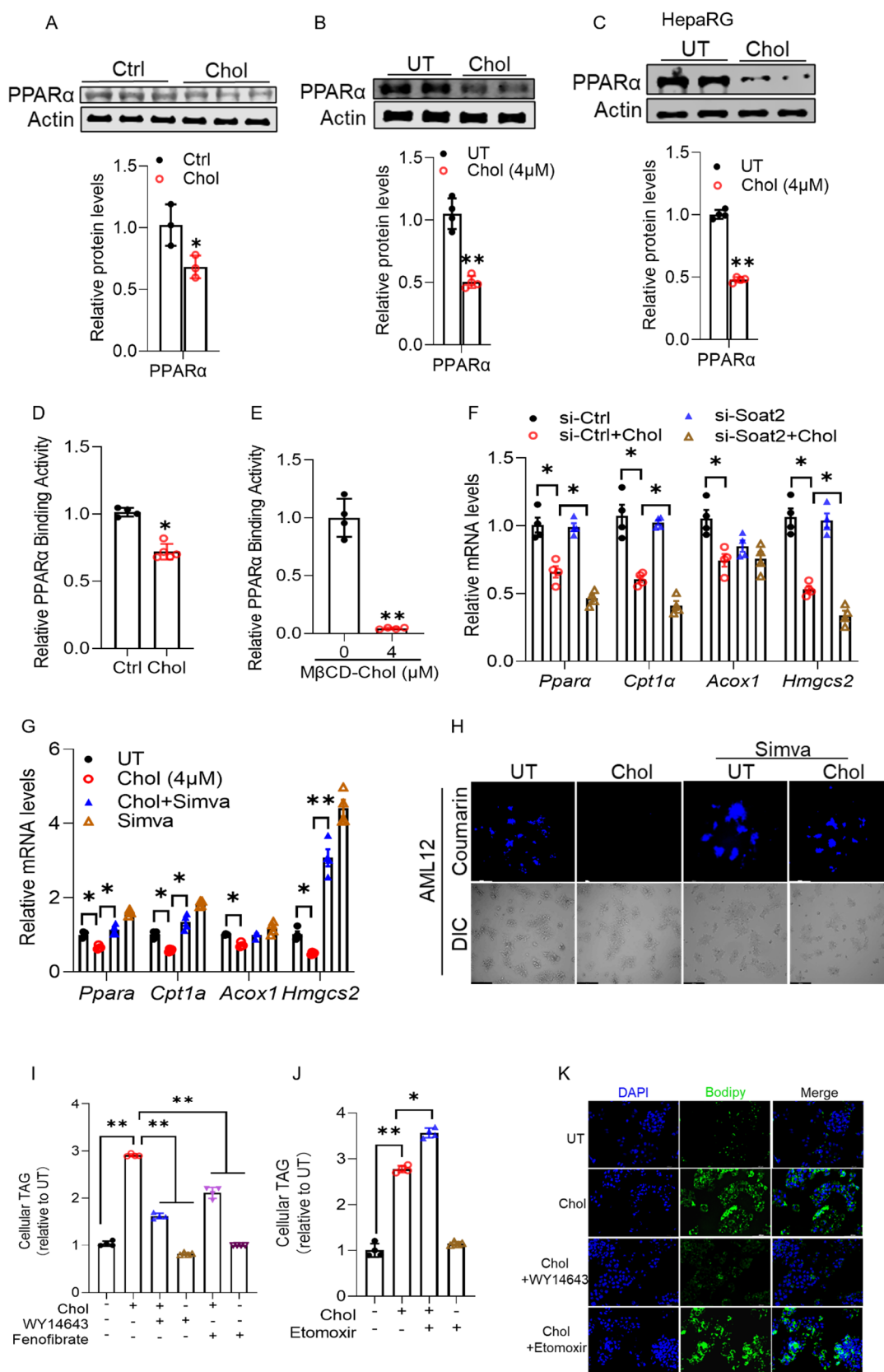


**Figure 3. Hepatocellular free cholesterol overload suppresses PPARα signaling, contributing to intracellular lipid accumulation.** Cholesterol-fed mice and MβCD-cholesterol-treated hepatocytes were examined for PPARα signaling. (A-C) Western blot analysis of PPARα protein levels in livers of cholesterol-fed mice and in AML12 and HepaRG cells exposed to cholesterol. (D, E) ELISA-based measurement of hepatic and cellular PPARα transcriptional activity. (F) qRT-PCR analysis of PPARα target genes in AML12 cells following siRNA-mediated *Soat2* knockdown prior to cholesterol loading. (G) Effects of simvastatin (10 μM) pretreatment on PPARα protein expression and target gene induction in cholesterol-treated AML12 cells. (H) FAOBlue™ assay showing restoration of mitochondrial fatty acid β-oxidation by simvastatin in AML12 cells. (I) Intracellular TAG in AML12 cells treated with WY14643 or fenofibrate during cholesterol loading. (J) TAG accumulation in AML12 cells treated with the FAO inhibitor etomoxir. (K) BODIPY staining showing reduced lipid droplets with WY14643 and increased droplets with etomoxir. Scale bar=50 μm. Chol, cholesterol; MβCD-Chol, MβCD-cholesterol; Simva, simvastatin. \*P < 0.05 and \*\*P < 0.01 represent statistical significance.

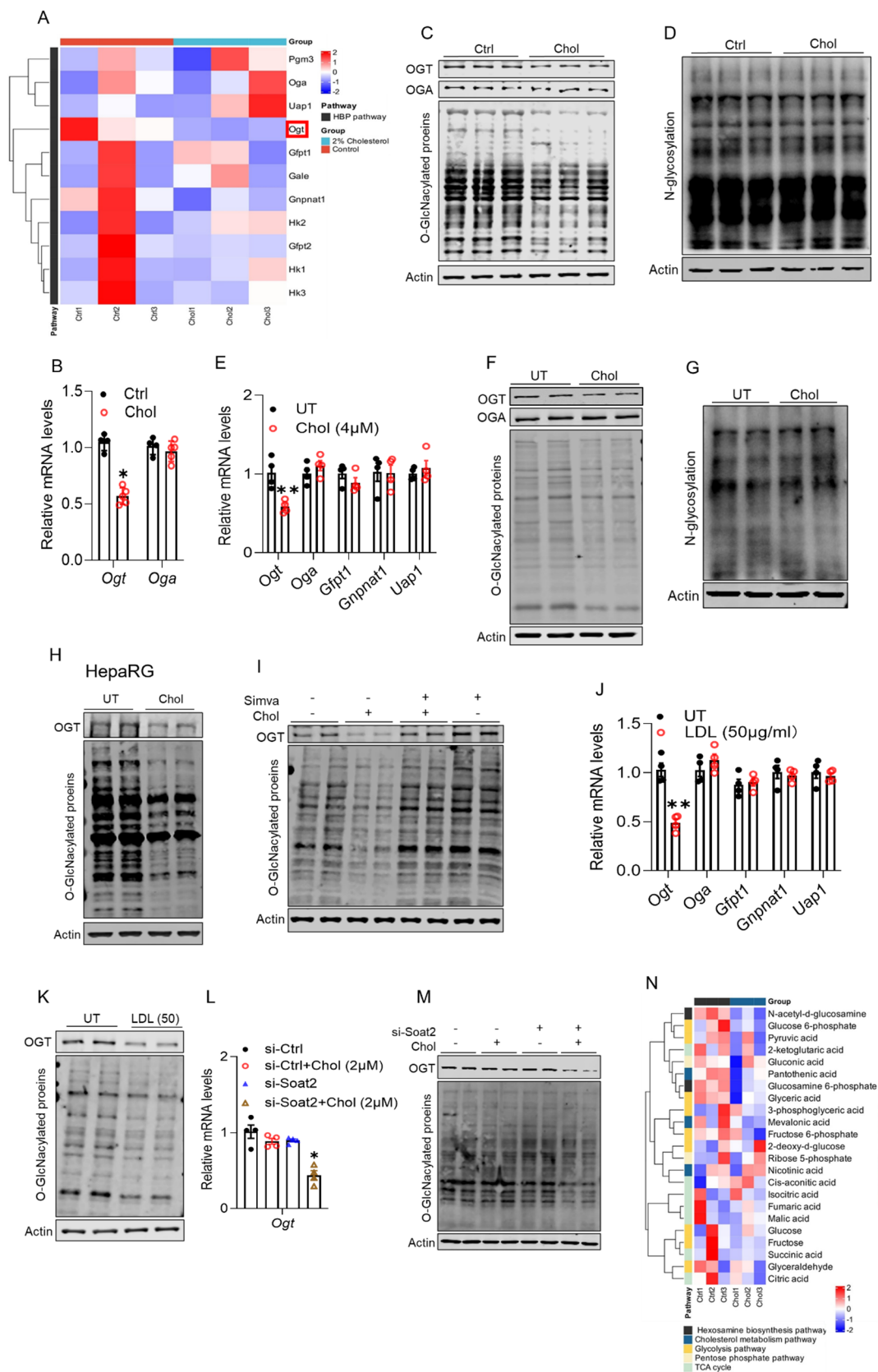


**Figure 4. Cholesterol loading downregulates hepatic OGT expression and suppresses hepatic protein O-GlcNAcylation.** Male C57BL/6j mice (10-week-old) were fed with a chow diet supplemented with and without cholesterol (2%, w/w) for 4 weeks. **(A)** Heatmap of transcriptomic profiling. **(B, C)** Validation by qRT-PCR and Western blot. **(D)** Lectin blot analysis showing unchanged N-linked glycosylation in the same samples. AML12 cells were treated with methyl- $\beta$ -cyclodextrin (M $\beta$ CD)-complexed cholesterol for 16 hours. **(E-G)** Validation by qRT-PCR and Western blot. **(H)** A similar result was observed in HepaRG cells. **(I)** Simvastatin (10  $\mu$ M, pretreatment for 2 h) reversed the cholesterol-induced reduction of OGT and global O-GlcNAcylation in AML12 cells. **(J, K)** LDL supplementation (50  $\mu$ g/mL, 16 h) decreased OGT mRNA and protein levels and suppressed O-GlcNAcylation in AML12 cells. **(L, M)** siRNA-mediated knockdown of *Soat2* further suppressed OGT expression and exacerbated the cholesterol (M $\beta$ CD-cholesterol, 2  $\mu$ M, 16 h)-induced decrease in global O-GlcNAcylation in AML12 cells. **(N)** Targeted metabolomic analysis of liver tissues. Chol, cholesterol; O-GlcNAc, O-GlcNAcylation. \* $P < 0.05$  and \*\* $P < 0.01$  represent statistical significance.

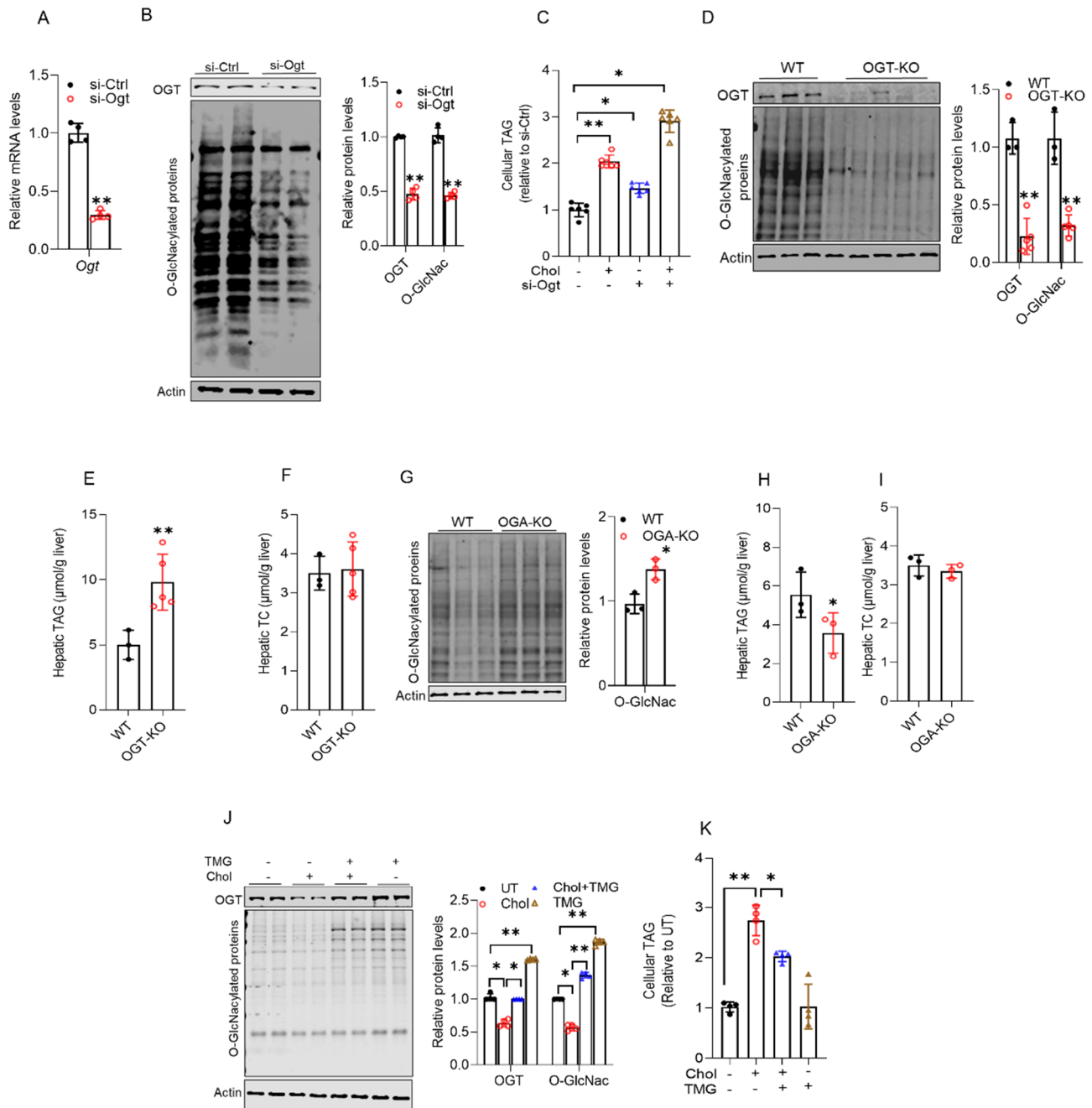


**Figure 5. Impairment of O-GlcNAcylation underlies cholesterol-induced hepatic fat accumulation.** AML12 cells were transfected with siRNA targeting *Ogt* overnight and then treated with methyl-β-cyclodextrin-cholesterol (4 μM, 16 h). (A) hepatic *Ogt* mRNA. (B) global protein O-GlcNAcylation and OGT protein; (C) cellular TAG content. Liver-specific *Ogt* or *Oga* knockout mice were used to examine *in vivo* effects. (D) hepatic global protein O-GlcNAcylation and OGT protein; (E) hepatic TAG; (F) hepatic TC; (G) hepatic global protein O-GlcNAcylation; (H) hepatic TAG; (I) hepatic TC. AML12 cells were pretreated with TMG for 2 hours prior to cholesterol loading. (J) global protein O-GlcNAcylation and OGT protein; (K) cellular TAG. Chol, cholesterol; O-GlcNAc, O-GlcNAcylation. \**P* < 0.05 and \*\**P* < 0.01 represent statistical significance.

**Impairment of O-GlcNAcylation underlies cholesterol-induced hepatic fat accumulation.** To determine whether cholesterol-induced OGT downregulation and subsequent suppression of protein O-GlcNAcylation contribute to hepatic lipid accumulation, we first inhibited OGT activity in hepatocytes using siRNA-mediated knockdown. OGT downregulation markedly reduced global protein O-GlcNAcylation, which was accompanied by a

significant increase in cellular TAG content in both AML12 (Figs. 5A-C) and HepG2 cells (Figs. S4A, B). Consistently, hepatocyte-specific OGT knockout mice exhibited inhibited hepatic protein O-GlcNAcylation (Fig. 5D), concomitant with pronounced TAG accumulation, without changes in hepatic TC levels (Figs. 5E, F). In contrast, hepatocyte-specific OGA knockout mice, in which protein O-GlcNAcylation is elevated (Fig. 5G), manifested reduced TAG levels

while maintaining normal hepatic TC content (Figs. 5H, I). Together, these findings demonstrate that OGT-mediated protein O-GlcNAcylation plays a critical role in maintaining hepatic lipid homeostasis. To further test this mechanism, we pharmacologically enhanced O-GlcNAcylation prior to cholesterol loading by pretreating AML12 and HepG2 cells with Thiamet-G (TMG), an OGA inhibitor that prevents O-GlcNAc removal from proteins. In line with prior observations, cholesterol exposure markedly decreased global protein O-GlcNAcylation in both cell types, and this effect was effectively reversed by TMG pretreatment (Fig. 5J and Fig. S4C). Importantly, restoration of O-GlcNAcylation significantly attenuated cholesterol-induced TAG accumulation (Fig. 5K and Fig. S4D).

**OGT-mediated O-GlcNAcylation is essential for hepatic PPAR $\alpha$  transactivation.** Our data show that hepatocellular cholesterol overload inhibits both PPAR $\alpha$  transactivation and OGT-mediated protein O-GlcNAcylation, and that these impairments contribute to hepatic lipid accumulation. These findings led us to hypothesize that PPAR $\alpha$  transactivity is regulated by protein O-GlcNAcylation. To explore this potential link, we manipulated OGT and OGA expression and activity using both pharmacological and genetic approaches in cultured hepatocytes and subsequently assessed PPAR $\alpha$  transactivity. As shown in Figs. 6A-C, the OGT inhibitor (OSMI) reduced PPAR $\alpha$  expression at both the mRNA and protein levels, accompanied by a coordinated downregulation of canonical PPAR $\alpha$  target genes, including those involved in mitochondrial  $\beta$ -oxidation. Importantly, co-treatment with the OGA inhibitor, TMG (10  $\mu$ M), restored OSMI-suppressed PPAR $\alpha$  expression (Fig. 6B). Similar findings were observed in HepG2 cells (Fig. 6C). Consistently, genetic inhibition of *Ogt* via siRNA transfection recapitulated the effects of pharmacological inhibition on *Ppara* expression and its canonical downstream targets (Fig. 6D). This observation was further supported by a direct ELISA-based transactivity assay (Fig. 6E), as well as reduced fatty acid  $\beta$ -oxidation, as evidenced by FAOBlue staining in cultured hepatocytes (Figs. 6F, G). Co-immunoprecipitation (CO-IP) revealed that PPAR $\alpha$  physically interacts with OGT and is directly O-GlcNAcylated (Fig. 6H), indicating a potential post-translational regulatory mechanism. Lastly, to establish *in vivo* relevance, we assessed hepatic PPAR $\alpha$  activity in liver-specific OGT-deficient mice. In line with our cell-based findings, hepatic *Ogt* deficiency reduced *Ppara* expression and its canonical

downstream targets (Fig. 6I). In contrast, *Oga* knockout in mice led to an opposite transcriptional pattern, as evidenced by increased expression of *Ppara* and its downstream targets (Fig. 6J). Collectively, these data identify OGT-mediated protein O-GlcNAcylation as a key mechanism required to sustain PPAR $\alpha$  transactivation.

**Either the improvement of protein O-GlcNAcylation or PPAR $\alpha$  activation attenuates cholesterol-induced hepatic steatosis.** To evaluate the translational relevance of our mechanistic findings, we investigated whether cholesterol diet-induced hepatic steatosis can be ameliorated by enhancing protein O-GlcNAcylation or by pharmacological activation of PPAR $\alpha$  in mice. To this end, 10-week-old male C57BL/6 mice were fed a 2% cholesterol-supplemented diet for 30 days and received a single retro-orbital injection of either AAV8-shScramble or AAV8-shOga on day 10 to increase hepatic O-GlcNAcylation via OGA knockdown. AAV8-shOga delivery effectively reduced hepatic OGA expression and ameliorated cholesterol-induced inhibition of protein O-GlcNAcylation (Figs. 7A, B), which was associated with marked improvements in cholesterol-induced hepatic abnormalities, including decreased fat accumulation (Figs. 7C, D), reduced liver weight (Fig. 7E), and a lower liver-to-body weight ratio (Fig. 7F), without affecting hepatic total cholesterol levels (Fig. 7G). To assess whether pharmacological activation of PPAR $\alpha$  could rescue MASLD progression, male C57BL/6 mice were fed a high-fat diet (HF; 35% kcal from fat) supplemented with 2% (w/w) cholesterol (HFC) for 6 weeks. WY14643 (30 mg/kg/day) was administered beginning in week 4 and continued throughout the final three weeks of dietary challenge. WY14643 treatment robustly activated hepatic PPAR $\alpha$  signaling, as evidenced by upregulation of canonical PPAR $\alpha$  target genes (Fig. 7H) and enhanced nuclear PPAR $\alpha$  transactivation (Fig. 7I). Restoration of PPAR $\alpha$  function was associated with a marked improvement in the hepatic phenotype, including reduced liver weight and the liver-to-body weight ratio (Figs. 7J, K), as well as decreased plasma ALT levels (Fig. 7L), indicating attenuated hepatocellular injury. Both hepatic (Fig. 7M) and circulating TAG concentrations (Fig. 7N) were significantly reduced, while total cholesterol levels in the liver and plasma remained unchanged (Figs. 7O, P), suggesting that the therapeutic benefits of PPAR $\alpha$  activation were independent of systemic cholesterol burden.

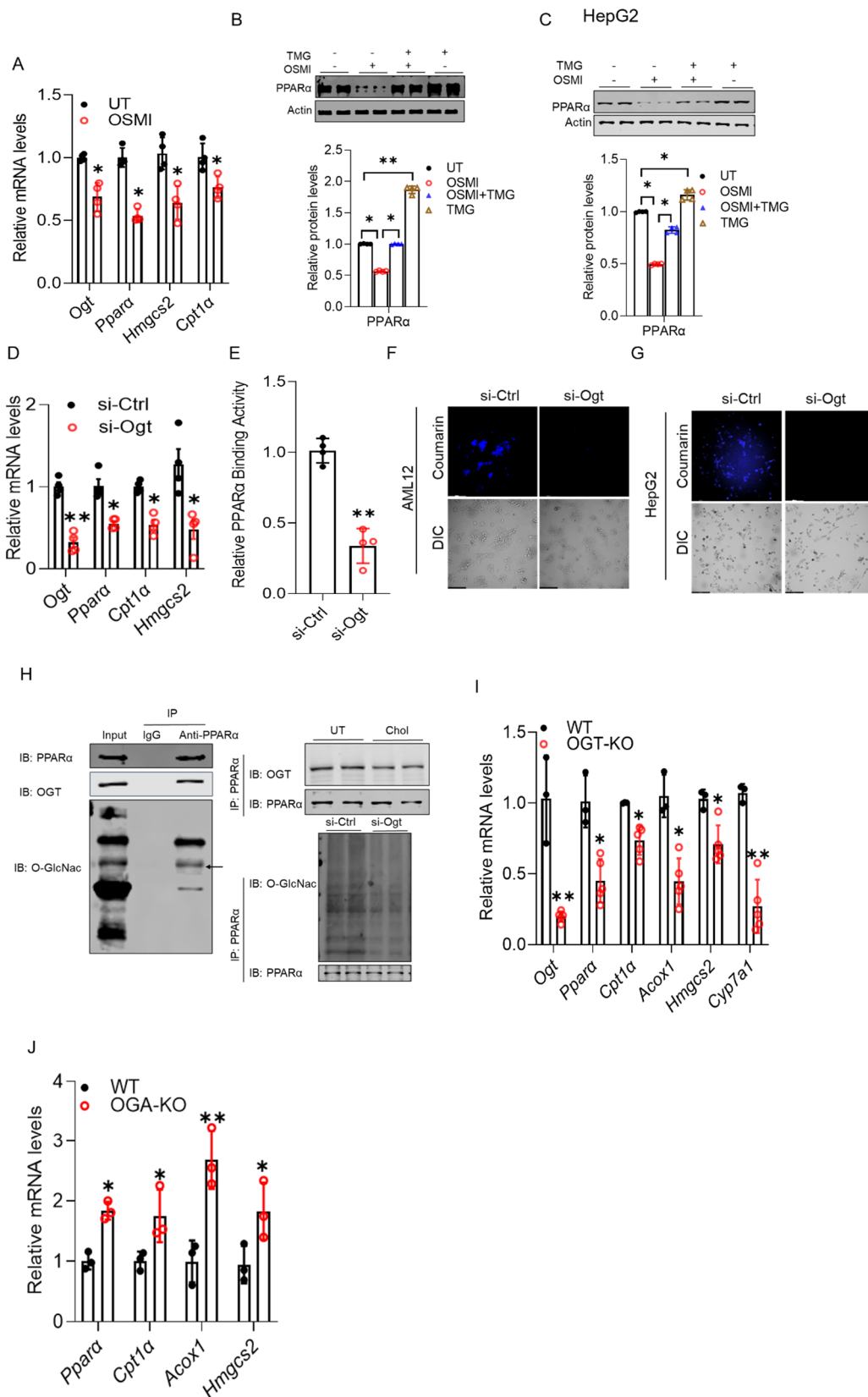


**Figure 6. OGT-mediated O-GlcNAcylation is essential for hepatic PPARα transactivation.** AML12 cells were treated with OSMI-1. (A) qRT-PCR analysis of *Ogt*, *Ppara*, *Hmgcs2*, and *Cpt1a* mRNA levels. AML12 and HepG2 cells were treated with OSMI-1, either alone or in combination with TMG. (B, C) Western blot analyses of PPARα protein. (D, E) qRT-PCR and ELISA analyses showing that *Ogt* silencing reduced *Ppara*, *Hmgcs2*, and *Cpt1a* expression and decreased PPARα transcriptional activity in AML12 cells. (F, G) FAOBlue™ assay in AML12 and HepG2 cells. PPARα O-GlcNAcylation was examined by co-immunoprecipitation. (H) OGT association with PPARα (IB: OGT) and O-GlcNAcylation of PPARα (IB: O-GlcNAc; arrow). Right: effects of cholesterol treatment or siOgt on PPARα O-GlcNAcylation. (I, J) qRT-PCR analysis of hepatic *Ppara*, *Hmgcs2*, *Cpt1a*, *Acox1*, and *Cyp7a1* mRNA levels in liver-specific OGT- and OGA-deficient mice. O-GlcNAc, O-GlcNAcylation. \* $P < 0.05$  and \*\* $P < 0.01$  represent statistical significance.

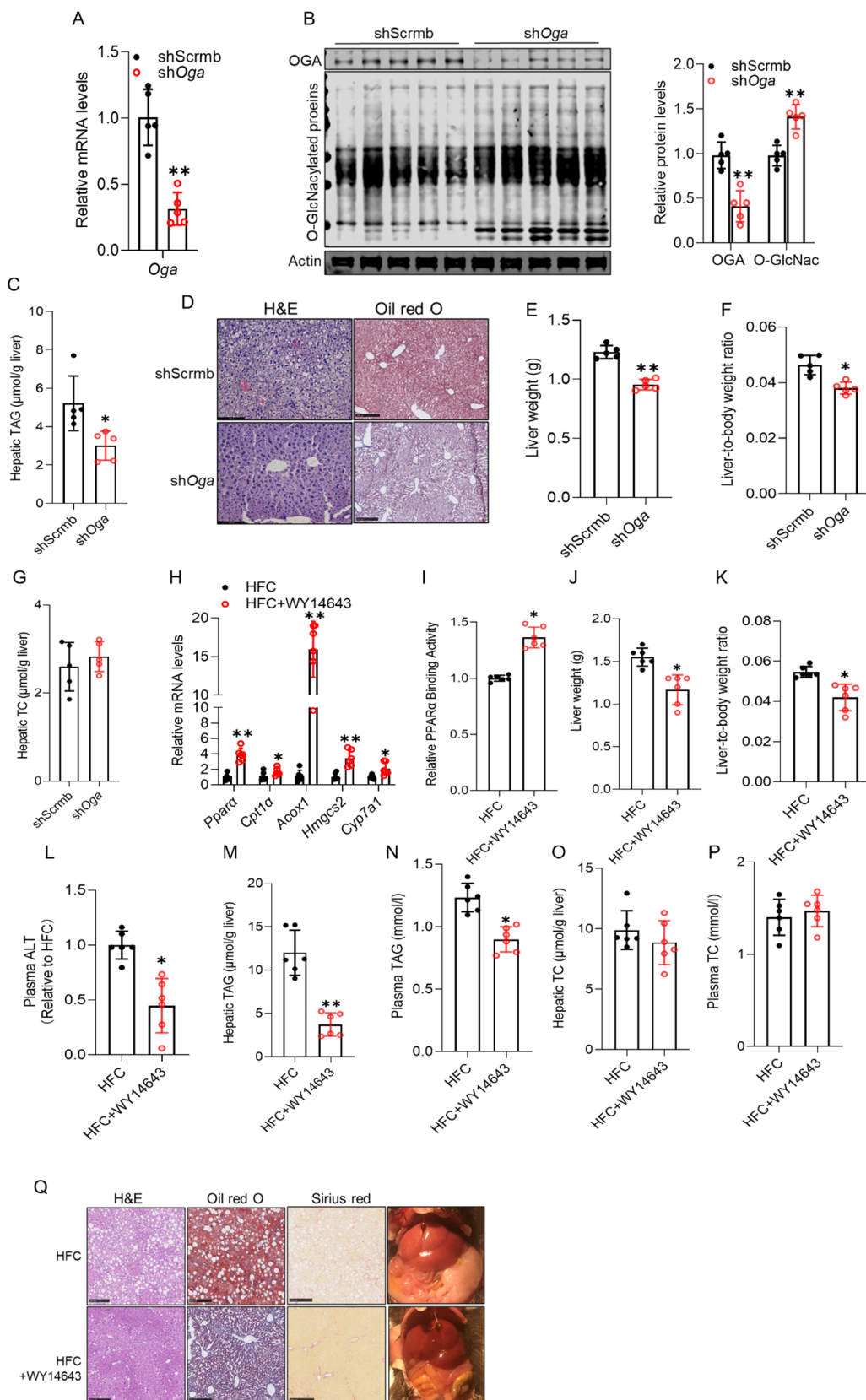


**Figure 7. Either the improvement of protein O-GlcNAcylation or PPAR $\alpha$  activation attenuates cholesterol-induced hepatic steatosis.** C57BL/6 male mice (10-week-old) were fed a 2% cholesterol diet for 30 days. On day 10, mice received a single retro-orbital injection of AAV8-shScramble or AAV8-shOga. **(A)** hepatic *Oga* mRNA; **(B)** hepatic OGA protein and global protein O-GlcNAcylation; **(C)** hepatic TAG; **(D)** representative liver images, H&E and Oil Red O staining; **(E)** liver weight; **(F)** liver-to-body weight ratio; **(G)** hepatic TC. C57BL/6 mice fed a high-fat diet supplemented with 2% cholesterol (HFC) and treated with WY14643. **(H)** hepatic mRNA expression of canonical *Ppar $\alpha$*  target genes; **(I)** Nuclear PPAR $\alpha$  transactivation; **(J)** liver weight; **(K)** liver-to-body weight ratio; **(L)** Plasma alanine aminotransferase (ALT) levels; **(M, N)** hepatic and plasma TAG; **(O, P)** hepatic and plasma TC; **(Q)** representative liver morphology and histological analyses (H&E, Oil Red O, and Sirius Red staining. Chol, cholesterol; O-GlcNAc, O-GlcNAcylation. Chol, cholesterol; M $\beta$ CD-Chol, M $\beta$ CD-cholesterol; Simva, simvastatin. \* $P < 0.05$  and \*\* $P < 0.01$  represent statistical significance.

Histological analyses, including H&E, Oil Red O, and Sirius Red staining, further confirmed the protective role of PPAR $\alpha$  activation (Fig. 7Q). Consistently, gross examination also confirmed improved liver appearance in WY14643-treated mice.

**SREBP2 regulates OGT expression and mediates cholesterol-induced suppression of protein O-GlcNAcylation and PPAR $\alpha$  signaling.** To elucidate the molecular mechanism underlying cholesterol-induced OGT suppression, we performed an integrative analysis combining RNA-seq-derived transcriptomic data with JASPAR transcription factor binding predictions. This analysis identified sterol regulatory element-binding protein 2 (SREBP2) as a putative transcriptional regulator of *Ogt* (Fig. 8A). Consistent with RNA-seq data (Fig. 8B), cholesterol loading via either M $\beta$ CD-cholesterol or LDL treatment consistently inhibited SREBP2 activation across all hepatocyte models used in this study and liver tissues (Figs. 8C-E and Figs. S5A, B). To assess the functional relevance of SREBP2, we silenced *Srebf2* in AML12 and HepG2 cells using siRNA (Figs. 8F, G, and Fig. S5C). *Srebf2* knockdown increased intracellular fat accumulation under basal conditions, which was further exacerbated by cholesterol loading (4  $\mu$ M) (Fig. 8H and Fig. S5D). This phenotype was accompanied by reduced OGT expression, decreased global protein O-GlcNAcylation, and impaired PPAR $\alpha$  signaling, as reflected by reduced PPAR $\alpha$  protein abundance and transcriptional activity (Figs. 8I, J, and Fig. S5E), along with downregulation of canonical PPAR $\alpha$  target genes (Fig. 8K). Functionally, *Srebf2* silencing markedly decreased fatty acid oxidation (FAO) capacity, an effect that was partially rescued by WY14643, a selective PPAR $\alpha$  agonist (Fig. 8L and Fig. S5F). To determine whether SREBP2 directly regulates *Ogt* transcription, we performed chromatin immunoprecipitation (ChIP) using primers targeting the -2 kb region upstream of the *Ogt* transcription start site, where SREBP2 binding motifs were predicted. ChIP-qPCR analysis confirmed direct binding of SREBP2 to the *Ogt* promoter (Fig. 8M). Collectively, these findings identify SREBP2 as a direct transcriptional activator of OGT and demonstrate that cholesterol suppresses hepatic OGT expression by inhibiting SREBP2 activity. This repression impairs O-GlcNAc-dependent mitochondrial fatty acid  $\beta$ -oxidation, at least in part by inhibiting PPAR $\alpha$  signaling.

## Discussion

Although dietary cholesterol has long been implicated in MASLD progression [8, 44], whether and

how cholesterol loading drives hepatocellular fat accumulation has remained unclear. Here, we identify a previously unrecognized mechanism by which free cholesterol promotes hepatic steatosis by suppressing PPAR $\alpha$ -dependent fatty acid  $\beta$ -oxidation. Mechanistically, hepatocellular cholesterol overload downregulates OGT expression, leading to reduced global protein O-GlcNAcylation, including that of PPAR $\alpha$ . This loss of O-GlcNAcylation impairs PPAR $\alpha$  transactivity, thereby compromising mitochondrial fatty acid  $\beta$ -oxidation and promoting intracellular lipid accumulation. Importantly, restoration of protein O-GlcNAcylation via hepatic OGA knockdown or pharmacological activation of PPAR $\alpha$  effectively attenuated cholesterol-induced steatosis in both cultured hepatocytes and mouse models (Fig. 8N). Collectively, these findings establish a cholesterol-OGT-O-GlcNAc-PPAR $\alpha$  axis linking cholesterol overload to impaired fatty acid oxidation and hepatic steatosis and highlight O-GlcNAc signaling and PPAR $\alpha$  as promising therapeutic targets.

Although dietary cholesterol is well recognized as a major driver of advanced MASLD, contributing to inflammation, liver injury, and fibrosis, collectively termed cholesterol-associated steatohepatitis (CASH) [8, 45-47], its role in promoting hepatocellular fat accumulation and hepatic steatosis, the earliest stage of MASLD, has remained poorly defined. Our findings address this gap using both *in vivo* and *in vitro* models. In cell culture studies, we demonstrate that exogenous cholesterol, supplied either as free cholesterol (M $\beta$ CD-cholesterol) or in its physiologically relevant LDL-bound form, is sufficient to induce hepatocellular fat accumulation independent of changes in *de novo* lipogenesis (DNL), adipose tissue lipolysis, or VLDL secretion. The specificity of this mechanism is supported by two key observations: (1) simvastatin treatment, which reduces intracellular cholesterol, markedly attenuates cellular fat accumulation under our experimental treatments; and (2) silencing of *Soat2*, which blocks cholesterol esterification and expands the free cholesterol pool, further exacerbates TAG accumulation. These effects were consistently observed across multiple hepatic models, including murine AML12, human HepG2, and HepaRG cells, and were validated in our animal studies, in which mice were fed cholesterol-supplemented chow or high-fat diets. Importantly, hepatic TAG accumulation increased in a dose-dependent manner with respect to cholesterol, without concurrent changes in body weight or systemic metabolic parameters, indicating a direct, liver-specific effect of cholesterol overload.

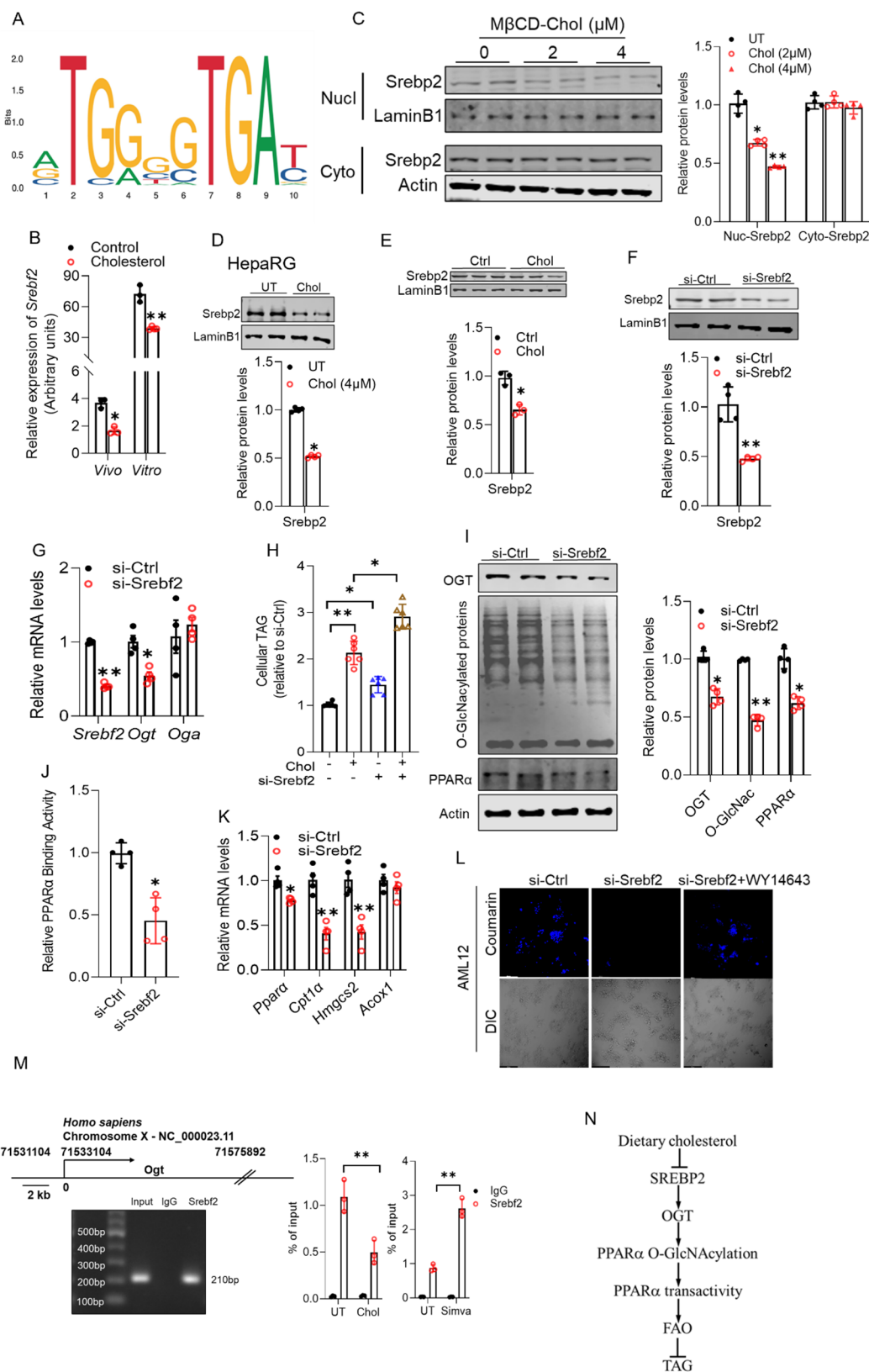


**Figure 8. SREBP2 regulates OGT expression and mediates cholesterol-induced suppression of protein O-GlcNAcylation and PPAR $\alpha$  signaling.** Integrative transcriptomic analysis was performed to identify transcriptional regulators of *Ogt*. (A, B) RNA-seq pathway analysis combined with JASPAR motif prediction identified SREBP-2 as a candidate regulator of *Ogt*. SREBP-2 expression in hepatocytes and mouse liver. (C-E) Western blot analysis of SREBP-2 protein in AML12 cells, HepaRG cells, and livers of cholesterol-fed mice. Functional analysis of *Srebf2* knockdown in AML12 cells treated with or without M $\beta$ CD-cholesterol. (F) Western blot of SREBP-2 protein; (G) qRT-PCR of *Srebf2*, *Ogt*, and *Oga*; (H) intracellular TAG content; (I) Western blot and quantification of global O-GlcNAcylation, OGT, and PPAR $\alpha$ ; (J) ELISA-based PPAR $\alpha$  transcriptional activity; (K) qRT-PCR of canonical PPAR $\alpha$  target genes. (L) FAOBlue™ assay showing FAO activity following *Srebf2* knockdown, with or without co-treatment with the PPAR $\alpha$  agonist WY14643. (M) ChIP-qPCR analysis demonstrates direct binding of SREBP-2 to the *Ogt* promoter (~2 kb upstream of the transcription start site). (N) Schematic summary of the proposed mechanism. Chol, cholesterol; O-GlcNAC, O-GlcNAcylation. \* $P < 0.05$  and \*\* $P < 0.01$  represent statistical significance.

Mechanistically, our study identifies mitochondrial fatty acid oxidation inhibition as a central driver of cholesterol-induced hepatocellular fat accumulation. To delineate the underlying mechanism, we focused on PPAR $\alpha$ , a key transcriptional regulator governing mitochondrial and peroxisomal  $\beta$ -oxidation. Our findings demonstrate that hepatocellular free cholesterol overload markedly suppresses PPAR $\alpha$  transactivation. This conclusion is supported by converging evidence, including reduced PPAR $\alpha$  expression, downregulation of canonical PPAR $\alpha$ -targeting genes, and direct measurements of diminished transcriptional activity. These data indicate that cholesterol accumulation disrupts PPAR $\alpha$ -dependent metabolic programming, thereby impairing fatty acid catabolism. Importantly, pharmacological activation of PPAR $\alpha$  using structurally distinct agonists effectively restored  $\beta$ -oxidation capacity and prevented lipid accumulation in cholesterol-overloaded hepatocytes. These results not only establish PPAR $\alpha$  inhibition as a key mechanistic link between cholesterol overload and defective fatty acid oxidation but also highlight PPAR $\alpha$  as a potential therapeutic target for mitigating cholesterol-driven hepatic steatosis.

Another interesting finding of the present study is that cholesterol overload suppresses OGT-mediated protein O-GlcNAcylation. To our knowledge, this is the first study to establish a direct association between hepatic cholesterol overload and OGT downregulation. O-GlcNAcylation is a reversible, nutrient-sensitive post-translational modification catalyzed by OGT and removed by OGA [29, 48]. Although O-GlcNAc signaling has been primarily studied in the context of glucose-responsive pathways such as SREBP-1c- and mTORC1-mediated lipogenesis [49, 50], its role in cholesterol-induced metabolic alterations has remained largely unexplored. Here, we demonstrate that intracellular cholesterol accumulation suppresses OGT expression at both the mRNA and protein levels, leading to global reductions in protein O-GlcNAcylation. Notably, these cholesterol-induced defects are functionally reversible; either pharmacological inhibition of OGA or genetic deletion of hepatic *Oga* restores global protein O-GlcNAcylation and alleviates cholesterol-induced steatosis. Conversely, hepatocyte-specific *Ogt* deletion phenocopies the metabolic effects of a cholesterol-enriched diet. Collectively, these findings define O-GlcNAc signaling as a critical regulatory axis linking cholesterol overload to hepatic steatosis.

The observation that hepatocellular free cholesterol overload is associated with both PPAR $\alpha$  inhibition and suppression of OGT-mediated protein O-GlcNAcylation prompted us to further explore the

mechanistic connection between O-GlcNAcylation and PPAR $\alpha$  transactivation. Our results identify PPAR $\alpha$  as a key downstream target whose activity is regulated by O-GlcNAcylation. PPAR $\alpha$  is a master transcriptional regulator of mitochondrial and peroxisomal  $\beta$ -oxidation pathways, and its activity is modulated by ligand binding, phosphorylation, and other post-translational modifications [10, 11, 16]. Our results demonstrate that O-GlcNAcylation positively regulates PPAR $\alpha$  transcriptional activity, providing an additional layer of control over hepatic lipid catabolism. Co-immunoprecipitation (Co-IP) confirmed that PPAR $\alpha$  is directly O-GlcNAcylated, and loss of this modification resulted in reduced DNA-binding affinity and diminished transcriptional activation of  $\beta$ -oxidation genes. Restoring protein O-GlcNAcylation reinstated PPAR $\alpha$  activity and fatty acid  $\beta$ -oxidation gene expression, linking O-GlcNAcylation status to hepatic fatty acid  $\beta$ -oxidation capacity.

Integrative transcriptomic and ChIP analyses identified SREBP2 as a direct transcriptional activator of *Ogt*, demonstrating that SREBP2 binds the *Ogt* promoter to regulate its expression. Both cholesterol loading in cultured hepatocytes and dietary cholesterol supplementation in mice suppressed hepatic SREBP2 activity, consistent with the canonical feedback regulation of cholesterol homeostasis [51, 52]. This repression provides a mechanistic explanation for the downregulation of OGT in cholesterol-overloaded livers, extending the functional repertoire of SREBP2 beyond cholesterol biosynthesis and positioning it upstream of a cholesterol-OGT-fatty acid  $\beta$ -oxidation axis that governs hepatic metabolic flexibility. This pathway defines a regulatory checkpoint through which cholesterol impairs mitochondrial fatty acid  $\beta$ -oxidation and promotes steatosis, independent of canonical lipogenic mechanisms. While our data establishes that exogenous or dietary cholesterol disrupts O-GlcNAcylation via SREBP2 inhibition, hepatic cholesterol can also accumulate through non-dietary mechanisms, including increased endogenous synthesis, impaired biliary excretion, or enhanced cholesteryl ester hydrolysis. A recent study further demonstrated that caspase-2-mediated SREBP2 activation, together with feedback circuits involving LATS2, sustains hepatic cholesterol accumulation [53]. Whether these alternative routes converge on the same SREBP2-OGT axis remains to be determined.

In summary, our study delineates a previously unrecognized mechanism underlying cholesterol-induced hepatocellular fat accumulation and hepatic steatosis. Cholesterol-mediated downregulation of OGT and consequent loss of protein O-GlcNAcylation

impair PPAR $\alpha$  transactivation, leading to the inhibition of mitochondrial fatty acid  $\beta$ -oxidation and subsequent hepatic fat accumulation. Importantly, restoring protein O-GlcNAcylation or pharmacologically activating PPAR $\alpha$  effectively reverses these metabolic defects, demonstrating the causal role of this pathway in the development of fatty liver. Unlike FFAs, which have long been recognized as the primary drivers of hepatic steatosis due to their direct contribution to TAG synthesis and lipotoxic effects, cholesterol is not a direct substrate for TAG synthesis. The present study provides evidence that, by inhibiting mitochondrial fatty acid oxidation, cholesterol can act in concert with FFAs, both elevated in MASLD, to promote hepatic lipid accumulation and synergistically contribute to the development and progression of MASLD. Collectively, our findings establish O-GlcNAc signaling as a central metabolic checkpoint linking cholesterol sensing to lipid oxidation and suggest that targeting OGT-mediated O-GlcNAcylation or PPAR $\alpha$  activation may represent promising therapeutic strategies for cholesterol-driven fatty liver disease.

## Abbreviations

FFAs: free fatty acids; MASLD: metabolic dysfunction-associated steatotic liver disease; OGT: O-linked N-acetylglucosamine transferase; OGA: O-GlcNAcase; PPAR $\alpha$ : peroxisome proliferator-activated receptor alpha; SREBP2: sterol regulatory element-binding protein-2; TAG: triacylglycerol; TC: total cholesterol; TMG: thiamet G; HBP: hexosamine biosynthetic pathway; FAO: fatty acid oxidation; ALT: alanine aminotransferase; ACAT2: alanine aminotransferase.

## Supplementary Material

Supplementary materials and methods, figures. <https://www.ijbs.com/v22p5615s1.pdf>

## Acknowledgements

### Funding

This work was funded in part by US NIH Grants NIAAA R01AA026603 (to Z.S.) and the Natural Science Foundation of Zhejiang Province Grant LQN25H260003 (to R.G.).

### Availability of data and materials

All data and materials are available.

### Ethics approval and consent to participate

All animal experiments were conducted with the approval of the Institutional Animal Care and Use Committee at the University of Illinois Chicago on 11

June 2022 (approval number: ACC-22-052), and in accordance with the rules of the Basel Declaration and "Guide for the Care and Use of Laboratory Animals," 8th Edition.

## Author contributions

Conceptualization: Z.S. and R.G. Methodology: R.G., Y.L., and Q.D. Software: R.G., X.D., and S.L. Validation: Z.S. and R.G. Investigation: R.G., Y.L., and Q.D. Resources: Z.S., C.S., and U.A. Data curation: R.G. and Y.L. Writing-original draft: Z.S. Writing-review and editing: Z.S. and R.G. Visualization: Y.J. and Z.S. Supervision: Y.J. and Z.S. Funding acquisition: Z.S. and R.G.

## Competing Interests

The authors have declared that no competing interest exists.

## References

- Chan WK, Chuah KH, Rajaram RB, Lim LL, Ratnasingam J, Vethakkan SR. Metabolic Dysfunction-Associated Steatotic Liver Disease (MASLD): A State-of-the-Art Review. *J Obes Metab Syndr.* 2023; 32: 197-213.
- Cusi K, Abdelmalek MF, Apovian CM, Balapattabi K, Bannuru RR, Barb D, et al. Metabolic Dysfunction-Associated Steatotic Liver Disease (MASLD) in People With Diabetes: The Need for Screening and Early Intervention. A Consensus Report of the American Diabetes Association. *Diabetes Care.* 2025; 48: 1057-82.
- Iturbe-Rey S, Maccali C, Arrese M, Aspichueta P, Oliveira CP, Castro RE, et al. Lipotoxicity-driven metabolic dysfunction-associated steatotic liver disease (MASLD). *Atherosclerosis.* 2025; 400: 119053.
- Van Rooyen DM, Larter CZ, Haigh WG, Yeh MM, Ioannou G, Kuver R, et al. Hepatic free cholesterol accumulates in obese, diabetic mice and causes nonalcoholic steatohepatitis. *Gastroenterology.* 2011; 141: 1393-403, 403 e1-5.
- Ma F, Longo M, Meroni M, Bhattacharya D, Paolini E, Mughal S, et al. EHBPI suppresses liver fibrosis in metabolic dysfunction-associated steatohepatitis. *Cell Metab.* 2025; 37: 1152-70 e7.
- Yang Z, Li A, Jiang Y, Maidaiti X, Wu Y, Jin Y. Global burden of metabolic dysfunction-associated steatotic liver disease attributable to high fasting plasma glucose in 204 countries and territories from 1990 to 2021. *Sci Rep.* 2024; 14: 22232.
- Zhang L, Shi Y, Liang B, Li X. An overview of the cholesterol metabolism and its proinflammatory role in the development of MASLD. *Hepatol Commun.* 2024; 8.
- Horn CL, Morales AL, Savard C, Farrell GC, Ioannou GN. Role of Cholesterol-Associated Steatohepatitis in the Development of NASH. *Hepatol Commun.* 2022; 6: 12-35.
- Malhotra P, Gill RK, Saksena S, Alrefai WA. Disturbances in Cholesterol Homeostasis and Non-alcoholic Fatty Liver Diseases. *Front Med (Lausanne).* 2020; 7: 467.
- Burri L, Thoresen GH, Berge RK. The Role of PPARalpha Activation in Liver and Muscle. *PPAR Res.* 2010; 2010.
- Antwi MB, Lefere S, Clarisse D, Koorneef L, Heldens A, Onghena L, et al. PPARalpha-ERRalpha crosstalk mitigates metabolic dysfunction-associated steatotic liver disease progression. *Metabolism.* 2025; 164: 156128.
- Kersten S. Integrated physiology and systems biology of PPARalpha. *Mol Metab.* 2014; 3: 354-71.
- Monroy-Ramirez HC, Galicia-Moreno M, Sandoval-Rodriguez A, Meza-Rios A, Santos A, Armendariz-Borunda J. PPARs as Metabolic Sensors and Therapeutic Targets in Liver Diseases. *Int J Mol Sci.* 2021; 22.
- Fougerat A, Bruse J, Polizzi A, Montagner A, Guillou H, Wahl W. Lipid sensing by PPARalpha: Role in controlling hepatocyte gene regulatory networks and the metabolic response to fasting. *Prog Lipid Res.* 2024; 96: 101303.
- Pawlak M, Lefebvre P, Staels B. Molecular mechanism of PPARalpha action and its impact on lipid metabolism, inflammation and fibrosis in non-alcoholic fatty liver disease. *J Hepatol.* 2015; 62: 720-33.
- van Raalte DH, Li M, Pritchard PH, Wasan KM. Peroxisome proliferator-activated receptor (PPAR)-alpha: a pharmacological target with a promising future. *Pharm Res.* 2004; 21: 1531-8.
- Theys C, Vanderhaeghen T, Van Dijk E, Peleman C, Scheepers A, Ibrahim J, et al. Loss of PPARalpha function promotes epigenetic dysregulation of lipid homeostasis driving ferroptosis and pyroptosis lipotoxicity in metabolic

- dysfunction associated Steatotic liver disease (MASLD). *Front Mol Med.* 2023; 3: 1283170.
18. Bougarne N, Weyers B, Desmet SJ, Deckers J, Ray DW, Staels B, et al. Molecular Actions of PPARalpha in Lipid Metabolism and Inflammation. *Endocr Rev.* 2018; 39: 760-802.
  19. Hardwick JP, Osei-Hyiaman D, Wiland H, Abdelmegeed MA, Song BJ. PPAR/RXR Regulation of Fatty Acid Metabolism and Fatty Acid omega-Hydroxylase (CYP4) Isozymes: Implications for Prevention of Lipotoxicity in Fatty Liver Disease. *PPAR Res.* 2009; 2009: 952734.
  20. Wan J, Wu X, Chen H, Xia X, Song X, Chen S, et al. Aging-induced aberrant RAGE/PPARalpha axis promotes hepatic steatosis via dysfunctional mitochondrial beta oxidation. *Aging Cell.* 2020; 19: e13238.
  21. Brocker CN, Patel DP, Velenosi TJ, Kim D, Yan T, Yue J, et al. Extrahepatic PPARalpha modulates fatty acid oxidation and attenuates fasting-induced hepatosteatosis in mice. *J Lipid Res.* 2018; 59: 2140-52.
  22. Ip E, Farrell G, Hall P, Robertson G, Leclercq I. Administration of the potent PPARalpha agonist, Wy-14,643, reverses nutritional fibrosis and steatohepatitis in mice. *Hepatology.* 2004; 39: 1286-96.
  23. Chen K, Li YH, Xu SQ, Hu SH, Zhang L. Protective Effects of Peroxisome Proliferator-Activated Receptor-alpha Agonist, Wy14643, on Hypoxia/Reoxygenation Injury in Primary Rat Hepatocytes. *PPAR Res.* 2012; 2012: 547980.
  24. Sahin C, Melanson JR, Le Billan F, Magomedova L, Ferreira TAM, Oliveira AS, et al. A novel fatty acid mimetic with pan-PPAR partial agonist activity inhibits diet-induced obesity and metabolic dysfunction-associated steatotic liver disease. *Mol Metab.* 2024; 85: 101958.
  25. Kumar M, Awasthi A, Dutta D, Joshi A, Sharma M. Fenofibrate in Metabolic Dysfunction-associated Steatotic Liver Disease: A Systematic Review and Meta-analysis. *Indian J Endocrinol Metab.* 2025; 29: 268-75.
  26. Bond MR, Hanover JA. A little sugar goes a long way: the cell biology of O-GlcNAc. *J Cell Biol.* 2015; 208: 869-80.
  27. Akella NM, Ciraku L, Reginato MJ. Fueling the fire: emerging role of the hexosamine biosynthetic pathway in cancer. *BMC Biol.* 2019; 17: 52.
  28. Boyd SS, Robarts DR, Nguyen K, Villar M, Alghusen IM, Kotulkar M, et al. Multi-omics after O-GlcNAc alteration identified cellular processes promoting aneuploidy after loss of O-GlcNAc transferase. *Mol Metab.* 2024; 90: 102060.
  29. Zhang K, Yin R, Yang X. O-GlcNAc: A Bittersweet Switch in Liver. *Front Endocrinol (Lausanne).* 2014; 5: 221.
  30. Zhu H, Zhao T, Zhao S, Yang S, Jiang K, Li S, et al. O-GlcNAcylation promotes the progression of nonalcoholic fatty liver disease by upregulating the expression and function of CD36. *Metabolism.* 2024; 156: 155914.
  31. Paneque A, Fortus H, Zheng J, Werlen G, Jacinto E. The Hexosamine Biosynthesis Pathway: Regulation and Function. *Genes (Basel).* 2023; 14.
  32. Lu P, Liu Y, He M, Cao T, Yang M, Qi S, et al. Cryo-EM structure of human O-GlcNAcylation enzyme pair OGT-OGA complex. *Nat Commun.* 2023; 14: 6952.
  33. Hou C, Li W, Li Y, Ma J. O-GlcNAcAtlas 4.0: An Updated Protein O-GlcNAcylation Database with Site-specific Quantification. *J Mol Biol.* 2025; 437: 169033.
  34. Mardones P, Quinones V, Amigo L, Moreno M, Miquel JF, Schwarz M, et al. Hepatic cholesterol and bile acid metabolism and intestinal cholesterol absorption in scavenger receptor class B type I-deficient mice. *J Lipid Res.* 2001; 42: 170-80.
  35. Robarts DR, Kotulkar M, Paine-Cabrera D, Venneman KK, Hanover JA, Zachara NE, et al. The essential role of O-GlcNAcylation in hepatic differentiation. *HepatoL Commun.* 2023; 7.
  36. Hu YJ, Zhang X, Lv HM, Liu Y, Li SZ. Protein O-GlcNAcylation: The sweet hub in liver metabolic flexibility from a (patho)physiological perspective. *Liver Int.* 2024; 44: 293-315.
  37. Lambert JE, Ramos-Roman MA, Browning JD, Parks EJ. Increased *de novo* lipogenesis is a distinct characteristic of individuals with nonalcoholic fatty liver disease. *Gastroenterology.* 2014; 146: 726-35.
  38. Yang F, Chen Y, Zheng G, Gu K, Fan L, Li T, et al. LIMA1 O-GlcNAcylation Promotes Hepatic Lipid Deposition through Inducing beta-catenin-Regulated FASN Expression in Metabolic Dysfunction-Associated Steatotic Liver Disease. *Adv Sci (Weinh).* 2025; 12: e2415941.
  39. Zhang B, Li MD, Yin R, Liu Y, Yang Y, Mitchell-Richards KA, et al. O-GlcNAc transferase suppresses necroptosis and liver fibrosis. *JCI Insight.* 2019; 4.
  40. Ortega-Prieto P, Parlati L, Benhamed F, Regnier M, Cavalcante I, Montabord M, et al. O-GlcNAc transferase acts as a critical nutritional node for the control of liver homeostasis. *JHEP Rep.* 2024; 6: 100878.
  41. Boren J, Taskinen MR. Metabolism of Triglyceride-Rich Lipoproteins. *Handb Exp Pharmacol.* 2022; 270: 133-56.
  42. Samuel VT, Shulman GI. Nonalcoholic Fatty Liver Disease as a Nexus of Metabolic and Hepatic Diseases. *Cell Metab.* 2018; 27: 22-41.
  43. Li Y, Song Q, Guo R, Qian Y, Jiang Y, Song Z. Glucose metabolism through the hexosamine biosynthetic pathway drives hepatic *de novo* lipogenesis via promoting N-linked protein glycosylation. *Am J Physiol Gastrointest Liver Physiol.* 2025; 328: G746-G59.
  44. Ioannou GN. The Role of Cholesterol in the Pathogenesis of NASH. *Trends Endocrinol Metab.* 2016; 27: 84-95.
  45. Wang X, Cai B, Yang X, Sonubi OO, Zheng Z, Ramakrishnan R, et al. Cholesterol Stabilizes TAZ in Hepatocytes to Promote Experimental Non-alcoholic Steatohepatitis. *Cell Metab.* 2020; 31: 969-86 e7.
  46. Goicoechea L, Conde de la Rosa L, Torres S, Garcia-Ruiz C, Fernandez-Checa JC. Mitochondrial cholesterol: Metabolism and impact on redox biology and disease. *Redox Biol.* 2023; 61: 102643.
  47. Mells JE, Fu PP, Kumar P, Smith T, Karpen SJ, Anania FA. Saturated fat and cholesterol are critical to inducing murine metabolic syndrome with robust nonalcoholic steatohepatitis. *J Nutr Biochem.* 2015; 26: 285-92.
  48. Harwood KR, Hanover JA. Nutrient-driven O-GlcNAc cycling - think globally but act locally. *J Cell Sci.* 2014; 127: 1857-67.
  49. Sodi VL, Bacigalupa ZA, Ferrer CM, Lee JV, Gocal WA, Mukhopadhyay D, et al. Nutrient sensor O-GlcNAc transferase controls cancer lipid metabolism via SREBP-1 regulation. *Oncogene.* 2018; 37: 924-34.
  50. Xu C, Pan X, Wang D, Guan Y, Yang W, Chen X, et al. O-GlcNAcylation of Raptor transduces glucose signals to mTORC1. *Mol Cell.* 2023; 83: 3027-40 e11.
  51. Liu S, Gao Y, Zhang L, Yin Y, Zhang W. Rspo1/Rspo3-LGR4 signaling inhibits hepatic cholesterol synthesis through the AMPKalpha-SREBP2 pathway. *FASEB J.* 2020; 34: 14946-59.
  52. Ozkan-Nikitars T, Grzesik DJ, Romano LEL, Chapple JP, King PJ, Shoulders CC. N-SREBP2 Provides a Mechanism for Dynamic Control of Cellular Cholesterol Homeostasis. *Cells.* 2024; 13.
  53. Aylon Y, Gershoni A, Rotkopf R, Biton IE, Porat Z, Koh AP, et al. The LATS2 tumor suppressor inhibits SREBP and suppresses hepatic cholesterol accumulation. *Genes Dev.* 2016; 30: 786-97.